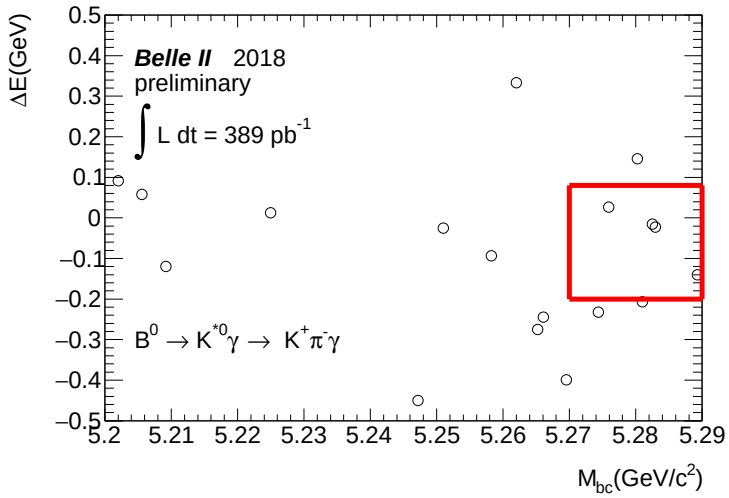

FIG. 1: Distribution of ΔE VS $M_{\rm bc}$ for $B^0 \to K^{*0}\gamma \to K^+\pi^-\gamma$ candidates in TOP-detector-calibrated 0.389 fb^{-1} out of 0.5 fb^{-1} of Phase II data. The red box corresponds to the signal box defined as $5.27\,\mathrm{GeV}/c^2 < M_{\rm bc} < 5.29\,\mathrm{GeV}/c^2$ and $-0.2\,\mathrm{GeV} < \Delta E < 0.08\,\mathrm{GeV}$. We find four signal candidates in the signal box.

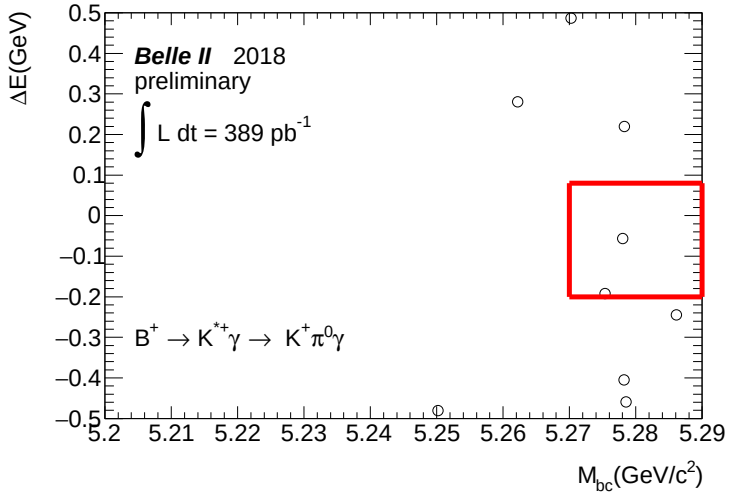

FIG. 2: Distribution of ΔE VS $M_{\rm bc}$ for $B^+ \to K^{*+}\gamma \to K^+\pi^0\gamma$ candidates in TOP-detector-calibrated 0.389 fb^{-1} out of 0.5 fb^{-1} of Phase II data. The red box corresponds to the signal box defined as $5.27\,\mathrm{GeV}/c^2 < M_{\rm bc} < 5.29\,\mathrm{GeV}/c^2$ and $-0.2\,\mathrm{GeV} < \Delta E < 0.08\,\mathrm{GeV}$. We find two signal candidates in the signal box.

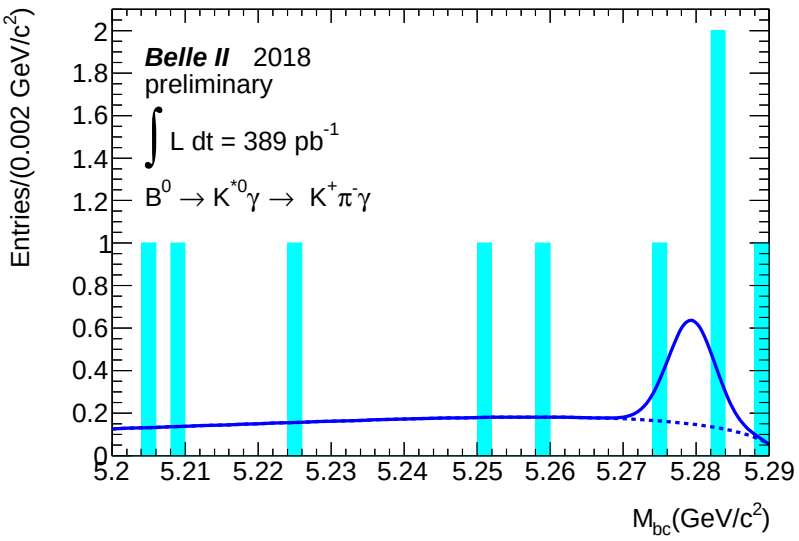

FIG. 3: Distribution of $M_{\rm bc}$ for $B^0 \to K^{*0}\gamma \to K^+\pi^-\gamma$ candidates in TOP-detector-calibrated 0.389 fb^{-1} out of 0.5 fb^{-1} of Phase II data. Blue line is the result of an extended unbinned maximum likelihood fit. Shape parameters of probability density functions are determined using signal and $q\bar{q}$ Monte-Carlo of the Phase II configuration.

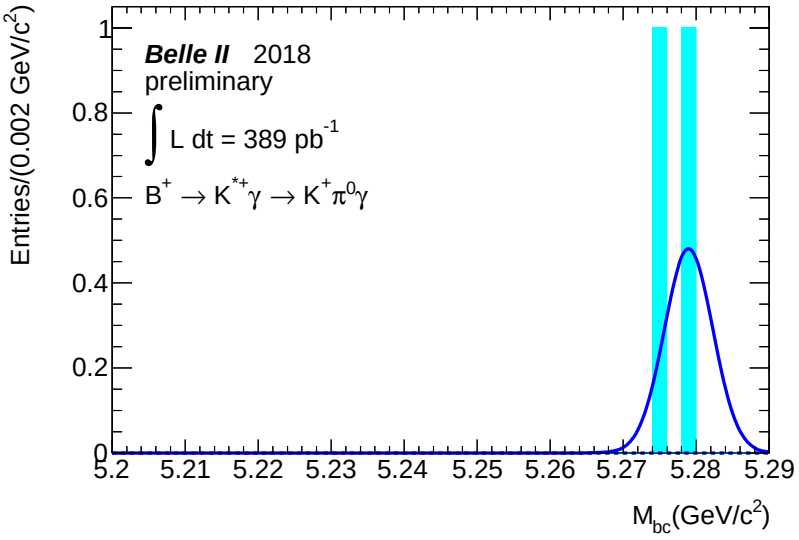

FIG. 4: Distribution of $M_{\rm bc}$ for $B^+ \to K^{*+}\gamma \to K^+\pi^0\gamma$ candidates in TOP-detector-calibrated 0.389 fb^{-1} out of 0.5 fb^{-1} of Phase II data. Blue line is the result of an extended unbinned maximum likelihood fit. Shape parameters of probability density functions are determined using signal and $q\bar{q}$ Monte-Carlo of the Phase II configuration.